CAMBRIDGE
UNIVERSITY PRESS

Highly sensitive RF sensor based on microstrip meander line for measuring microfluidics dielectric properties of alcohol–alcohol mixtures

Huan Zou[1] , Yiyun Wang[1], Xiaoqin Liu[1] and Haiyang Wang[2]

[1]School of Aeronautics and Astronautics, University of Electronic Science and Technology of China, Chengdu, Sichuan, China and [2]School of Electronic Science and Engineering (National Exemplary School of Microelectronics), University of Electronic Science and Technology of China, Chengdu, Sichuan, China

Abstract

In this paper, a radio frequency sensor for measuring microfluidics dielectric properties is designed based on microstrip meander line. The meander sensor replaces the straight transmission lines with meander transmission lines in the part of the half-wavelength path difference to improve the sensitivity of the sensor and reduce its size. According to the experimental results, the meander sensor based on the meander line has higher accuracy and a lower relative error than the straight sensor in measuring methanol–ethanol mixtures with different molar fractions. The relative error measured by the meander sensor after calibration with an adjustable cavity is less than 1%. It is easier to detect the very slight variation in dielectric properties brought about by microfluidics. The detection technique can be further applied for the accurate detection of dielectric properties of valuable biological samples, providing a more concise and convenient way.

Introduction

The study of the dielectric properties of trace substances has been a popular research topic in biomedical applications, such as studies of the normal and malignant breast tissues in xenograft mice [1], broadband dielectric properties of adrenal gland [2], and the dielectric properties of the bone at low frequencies [3]. The connection between electronics and life science has become increasingly close in recent years. The use of electronics to detect the electrical properties of biological samples and thus obtain their biological properties has become a fundamental and important measurement way. For example, biosensors [4–8] can detect changes in electrical signals caused by the changes in the concentration of a substance and thus obtain the properties of the substance itself or monitor its change process. The rampage of COVID-19 in 2019 has had a major impact on a wide range of industries. Biosensors can easily measure the electrical properties of viruses and their products [9–12] to obtain hidden signatures, which can be extremely beneficial for the rapid detection of viruses as well as for vaccine development. The microwave measurement is introduced into the design of biosensor, which can achieve nondestructive testing. The interferometer that uses microwave measurement to obtain dielectric properties of microfluidics can cancel the noise signal on the plane transmission line and thus improve the sensitivity of the sensor [13–15]. Chemical reagents are often used as test fluids to validate sensors [16, 17].

In order to improve the performance of the cancellation-type sensor, various improvements were proposed. In 2008, Song proposed a new approach for parasitic effects cancellation [18]. The method exploits the symmetry of two transmission channels on the chip to extract the changes of dielectric properties of microfluidics on two channels. The offset effect on simulation is better than 65 dB and then is optimized in subsequent work [19]. The coplanar waveguide transmission line structure has a high sensitivity [20–22]. Wideband [21, 23] and adjustable [22, 24–26] interferometers were designed to improve the sensitivity and detect fewer microfluidics changes. Adjustable sensors can reduce errors caused by machining, the dielectric substrate, and environmental factors by fine-tuning the electrical length and compensating transmission losses. But the sensitivity of the sensor with a small cavity is insufficient to detect more subtle changes in dielectric properties ($\Delta\varepsilon < 0.1$) of microfluids [22].

The introduction of the meander line into cancellation-type sensors (meander sensor) has the following advantages [21, 27–29]. First, the electrical field intensity is enhanced in the meander part and the interaction between the test branch and the microfluidics is increased

because of the meander line [27]. Second, the design of the meander line can increase the contact area between the microfluids under test and the meander part. Third, it can realize the miniaturization of the sensors [28]. Therefore, this paper analyzes the performance changes brought by meander sensor compared with that of traditional sensors with straight lines (straight sensor). The relation between the transmission parameters of the meander sensor and the dielectric properties of microfluidics is investigated in the next part of the paper. Then the simulation model of the meander sensor is constructed to measure the transmission coefficient of methanol–ethanol mixture with different molar fractions. Finally, the meander sensor machined according to the simulation model is used to test the complex permittivity of methanol–ethanol mixture at different molar fractions and compared with the tested values in the literature.

The design of meander sensor

The measurement principle of the cancellation-type sensor is that the signal is evenly divided into two signals with the same amplitude and phase after passing through the first Wilkinson power divider, one of which is 180° out of phase with the other after passing through an inverter, and the two signals with the same amplitude and opposite phase offset each other at the second Wilkinson power divider, which plays the role of power synthesis. The design schematic of the conventional cancellation-type sensor based on the microstrip line is shown in Fig. 1.

The measurement of straight sensor can be divided into three cases according to the analysis in [30].

(1) When the same substances are added to the test and reference segments and the losses of the straight sensor are not considered, the transmission coefficient can be expressed as

$$S_{21} = 0 \tag{1}$$

(2) When different substances are added to the test and reference segments and the losses of the straight sensor are not considered, the transmission coefficient can be expressed as [31]

$$
\begin{aligned}
S_{21} &= S_{21\_Ea} \times \Delta S_{21\_MUT} \\
&= S_{21\_Ea} \times \left(S_{21\_a} - S_{21\_b} \right) \\
&= S_{21\_Ea} \times \left[\frac{2Z_0}{2Z_0 + Z_a(\omega)} - \frac{2Z_0}{2Z_0 + Z_b(\omega)} \right] \\
&= 2AZ_0 S_{21\_Ea} j\omega C_l \times (\varepsilon_a - \varepsilon_b) \\
&= B(\varepsilon_a - \varepsilon_b)
\end{aligned} \tag{2}
$$

where ε_a and ε_b are the complex permittivity of microfluidics added to test branch and reference branch, C_l is the channel capacitance of the liquid, Z_0 is the characteristic impedance of the

transmission line and the impedance of the upper branch $Z_a = 1/\left(j\omega C_p + j\omega C_l \varepsilon_a\right)$, S_{21_Ea} represents the transmission coefficients of the remaining signal lines after removing l_a section, and S_{21_a} and S_{21_b} are the signal transmission coefficients of branch l_a and l_b. The different transmission coefficient of the upper and lower branches is ΔS_{21_MUT}.

(3) When different substances are added to the test and reference segments and the losses of the straight sensor are considered, the transmission coefficient can be expressed as

$$
\begin{aligned}
S_{21} &= S_{21\_Ea} \times \Delta S_{21\_MUT} + S_{21\_lad0} \\
&= 2AZ_0 S_{21\_Ea} j\omega C_l \times (\varepsilon_a - \varepsilon_b) + S_{21\_Ea}\left(\Delta C_l \varepsilon_a + \Delta C_p\right) \\
&\quad + \left(S_{21\_Ea} S_{21\_b} + S_{21\_Eb} S_{21\_a}\right)\left(C_l \varepsilon_a + C_p\right) \\
&= M\varepsilon_a - N\varepsilon_b + P
\end{aligned} \tag{3}
$$

The parameters M, N, and P can be obtained by calibrating sensor based on two microfluidics with known dielectric properties. When a microfluid of the same known dielectric parameter is placed at both the test branch l_a and the reference branch l_b of the sensor for calibration, $\varepsilon_a = \varepsilon_b$. The non-ideality of the power divider and synthesizer and the difference between the two channels are set to S_{21_lad0}, where $S_{21\_Ea}\left(\Delta C_l \varepsilon_a + \Delta C_p\right)$ indicates the transmission effect due to the difference in the materials added to the two branches and the unsatisfactory design of the power splitter. $\left(S_{21\_Ea} S_{21\_b} + S_{21\_Eb} S_{21\_a}\right)\left(C_l \varepsilon_a + C_p\right)$ indicates the transmission effect due to the difference between the two branches.

Equation (3) can be rewritten to $(S_{21})_b = M\varepsilon_b - N\varepsilon_b + P$. The material at the reference branch l_b remains unchanged, and the material at the test branch l_a is changed, $\varepsilon_a \neq \varepsilon_b$. Then $(S_{21})_a = M\varepsilon_a - N\varepsilon_b + P$. The parameters from Equation (3) can be approximated as constants when the dielectric properties of the microfluidics are varied in small ranges. Then $(S_{21})_a - (S_{21})_b = M(\varepsilon_a - \varepsilon_b)$, that is,

$$\Delta S_{21} = M\Delta\varepsilon \tag{4}$$

According to Equation (4), the dielectric parameter of the microfluidics at the test branch can be acquired by measuring the variation of the transmission parameters of the sensor. As can be seen in Fig. 1, the straight sensor is designed to achieve a 180° phase difference by extending the $\lambda/4$ path on each side of the test side. Now, this part is replaced by meander line, and the schematic of the meander sensor is shown in Fig. 2, where $l_a - l_b = 3\lambda/2$.

The derivation process of the meander sensor is like that of the straight sensor, which gives the relationship between the transmission parameters of the meander sensor and the microfluidics dielectric properties. The difference between two sensors comes from case 3. The introduction of meander line reduces impedance at the meander section and at the same time the length of the meander section is close to three times that of the straight section, which can be approximated by microwave theory
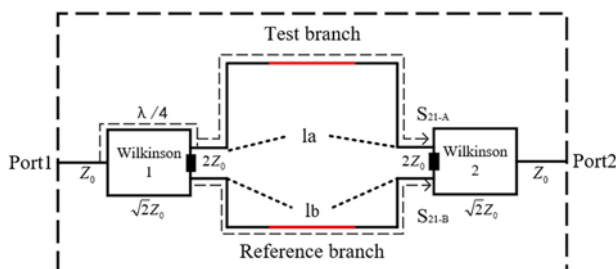

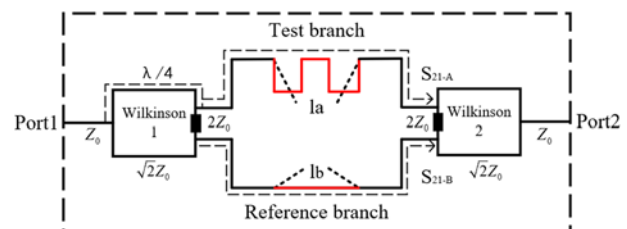**Figure 1.** The schematic of straight sensor.

Figure 2. The schematic of the meander sensor.

as $G_a(\omega) = 1/Z_a \approx (j\omega C_p + j\omega C_l \varepsilon_a)^3$. The materials added to the test branch and reference branch are not the same, as well as losses are considered. The non-ideality of the power dividers and the subtle differences of the two channels are set to S_{21_lad}. According to Equation (3), the transmission coefficient can be expressed as

$$
\begin{aligned}
S_{21} &= S_{21\_Ea} \times \Delta S_{21\_MUT} + S_{21\_lad} \\
&= S_{21\_Ea} \times (S_{21\_a} - S_{21\_b}) + S_{21\_lad} \\
&= S_{21\_Ea} \times \left[\frac{2Z_0}{2Z_0 + Z_a(\omega)} - \frac{2Z_0}{2Z_0 + Z_b(\omega)} \right] + S_{21\_lad} \\
&\approx U\varepsilon_a^3 - V\varepsilon_b + W
\end{aligned}
\tag{5}
$$

The introduction of meander line changes *R, L, C,* and *G* in the equivalent circuit, so that the impedance of the test branch decreases, which is about the third power of the reference branch after approximate analysis. After calibrating the sensor with two microfluidics of known dielectric parameters, there is

$$
\Delta S_{21} = U(\Delta\varepsilon)^3
\tag{6}
$$

When the dielectric parameters of materials in the test change in small ranges after calibration, the parameter *U* is regarded as a constant. However, when the dielectric parameters of materials in the test change far from the calibration value, the parameter *U* also gradually deviates from the constant value, leading to an increase in error. This is similar to the parameter *M* in the straight sensor. According to Equation (6), a larger variation of the transmission coefficient S_{21} is observed in Vector Network Analyzers after three amplifications. This proves that the meander sensor is easier for detecting small changes of the dielectric properties of microfluidics.

Comparative simulation analysis

The simulation models are constructed in Ansoft-HFSS according to above straight and meander sensor schematics, as shown in Fig. 3. The operating frequency of the sensors is 10 GHz, the dielectric substrate is Rogers 6010 with a relative permittivity of 10.2, the substrate thickness is 0.635 mm, and the microstrip line is 18 μm thick. The dielectric substrate and size are chosen to suppress the high frequency waveform and to avoid the deterioration of the transmission line performance. The operating frequency of the sensor is set at 10 GHz in order to achieve a compact design and reduce the amount of material to be measured at the meander section. Since chemical reagents are often used as test solutions for validating sensors, the dielectric parameters of methanol–ethanol

mixtures with different molar fractions in [16] are used as reference values in this paper. The methanol–ethanol mixture is added to the test branch in simulation to obtain the transmission coefficient S_{21} for the two sensors. The performance of the two sensors is compared based on the simulation results.

The cancellation-type sensor works by measuring the changes of the sensor transmission parameter S_{21} in response to the changes of the microfluidics dielectric properties. To measure the unknown dielectric parameters of microfluidics, two microfluidics with known dielectric parameters are required as calibration fluids to calibrate the two sensors and obtain the parameters *M* and *U*. Absolute methanol (0.4 μL) is placed at test and reference branch to calibrate. The straight sensor was calibrated to −108.72 dB at 10 GHz, and the meander sensor was calibrated to −105.78 dB at 9.95 GHz. Calibrating the two sensors to similar positions is to facilitate the comparative analysis later.

The material under reference branch is not changed, the material of test branch is replaced with the methanol–ethanol mixture with a molar fraction of 0.9 ($x_M = 0.9$). The ΔS_{21} obtained after calibration is substituted into Equations (4) and (6) to obtain the parameters *M* and *U*. Changing the solution at the test branch to methanol–ethanol mixture with different molarity ($x_M = 0.0 \sim 0.8$), the S_{21} values are obtained by simulation and then are compared with the calculated values through Equations (4) and (6) as shown in Fig. 4. The error between measured and calculated values is smaller for both the straight sensor and meander sensor, but the misclassification rate is higher for the straight sensor than that of the meander sensor. Since the meander sensor can widen the distance of transfer coefficient S_{21} between different molar fraction mixture, it makes the meander sensor more accurate in determining the molar fraction of the microfluidic mixture, and the meander sensor does not have the phenomenon that any subsequent determination will be wrong once there is a misjudgment.

Experiments

The design and implementation of sensors

The above simulation models are processed into two physical sensors, as shown in Fig. 5. In testing the sensor performance, chemical reagents are often used as test solutions for the sensor performance. The experiments are conducted with different molar fractions of the methanol–ethanol mixture as test solution to analyze the accuracy of the meander sensor in measuring the unknown microfluidics dielectric parameters. The dielectric parameters of
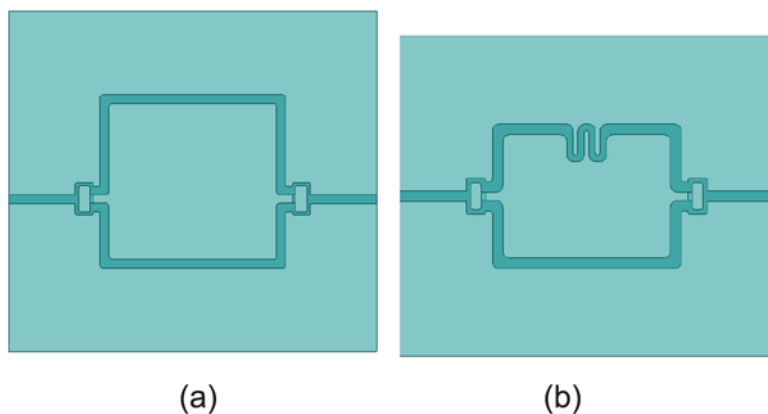

Figure 3. The simulation models of two different cancellation-type sensors: (a) straight sensor and (b) meander sensor.
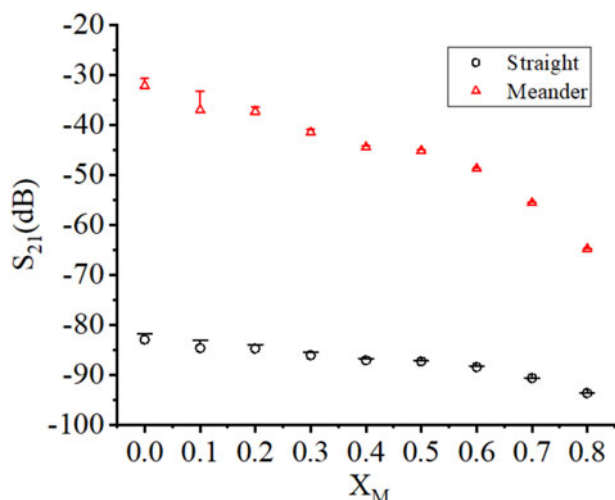
Figure 4. The contrastive analysis of simulation and calculation results of two sensors.
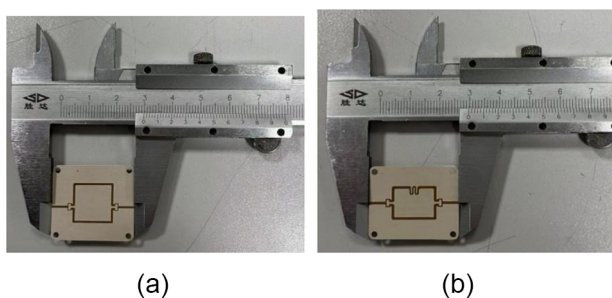

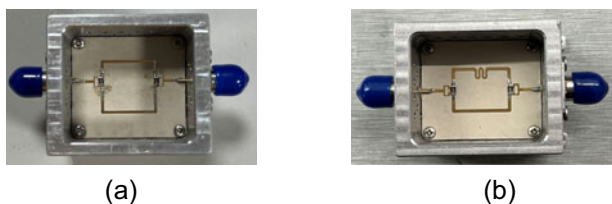**Figure 5.** Sensors without the adjustable cavity: (a) straight sensor and (b) meander sensor.

Figure 6. Sensors with the adjustable cavity. (a) Straight sensor with adjustable cavity but without shielding cover. (b) Meander sensor with adjustable cavity but without shielding cover. (c) Front view of the meander sensor with shield cover. (d) Side view of a meander sensor with shield cover.

methanol–ethanol mixtures with different molar fractions in [16] are used as reference values in this paper. This test is conducted in the room of 23°C, and the type of vector network analyzer is 3672C, and the sweep range is 9–11 GHz. Among the purchased absolute methanol (CH_3OH) content $\geq$ 99.5%, non-volatile is $\leq$ 0.001%.

For absolute ethanol (CH_3CH_2OH) mass fraction $\geq$99.7%, volatile residue mass fraction is 0.001%.

In order to fine-tune the electrical length, compensate for the losses and shield the interference from environment, and the adjustable cavity is designed in this paper to fine-tune the offset effect of the sensor. The sensor after adding the adjustable cavity is shown in Fig. 6. The offset effect of the sensor is adjusted by different positions, depths, and number of the screws, which is rotated into the thread holes on the cavity wall.

The size of the meander sensor without the adjustable cavity is 30 mm × 25 mm × 0.635 mm, which is smaller than that of straight sensor. The size of the meander sensor and the straight sensor with an adjustable cavity are 38 mm × 31 mm × 36 mm and 38 mm × 33 mm × 36 mm, respectively.

No-load and calibration testing of sensors

The vector network analyzer after calibrating is used to test the no-load condition of both sensors without placing microfluidics at the test and reference branches. The sensors are fine-tuned with the tuning screws and tuned to a better offset effect. The no-load test system of sensor with an adjustable cavity is shown in Fig. 7. When no test materials are loaded on the sensors, the S_{21} parameter of straight sensor at 9.88 GHz is −86.64 dB, the S_{21} parameter of the meander sensor at 9.94 GHz is −84.86 dB. Both sensors achieve good cancellation effect after fine-tuning with an adjustable cavity. An equal amount (0.4 μL) of absolute methanol solution is placed at the test and reference branch of the sensor using a micro-syringe, and the sensor is tuned to a better offset point with the help of an adjustable cavity. The test result of the meander sensor after calibration with absolute methanol solution is shown in Fig. 8. The offset effect of the meander sensor can reach −87.75 dB at 9.67 GHz and the offset effect of the straight sensor is −91.18 dB at 9.73 GHz.

The simulation and test results of the meander and straight sensors after calibration with absolute methanol are shown in Fig. 9. It can be seen from the graph that the test values differ from the simulation values by nearly 20 dB due to processing errors, the effects of welding, and air disturbance. The frequency shift occurs under the fine adjustment of the cavity.

The no-load and calibration results of the meander sensor designed in this paper were compared with the experimental results obtained by previous scholars, as shown in Table 1. Under
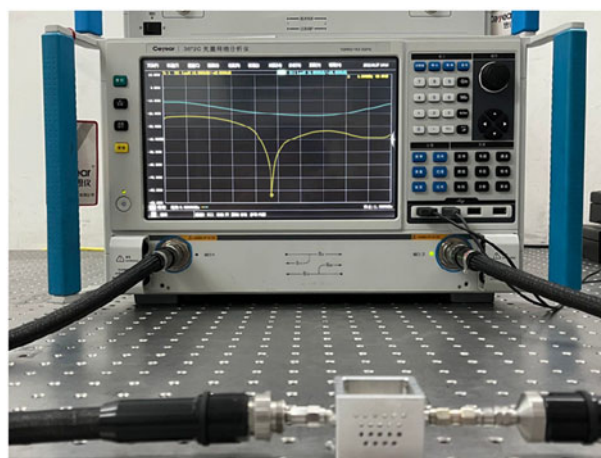

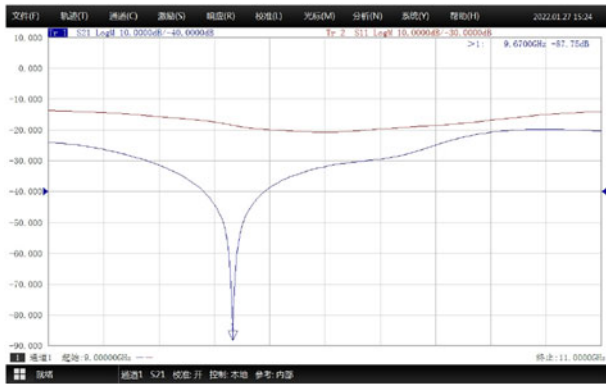**Figure 7.** No-load test system of meander sensor.

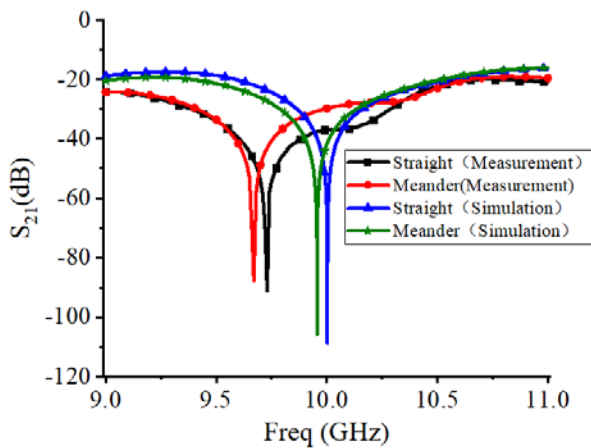**Figure 8.** *S*-parameters tested after calibration.

Figure 9. The simulation and test comparison chart of two sensors.

Table 1. Comparison table of no-load and calibration test results for different sensors

	No-load test (dB)	Calibration test (dB)
Song [17]	–	−56
Yang [18]	−80	−78
Liu [29]	–	−70
Wang [20]	−78	−71.88
This paper	−84.86	−87.75

the fine-tuning of an adjustable cavity with a shield cover, the offset effect of this paper is improved by more than 9 dB.

The test of minimum measurement volume for meander sensor

The volume of measured solution is tested to explore the effect of different solution volumes on the transmission parameters of the sensor, thus facilitating the control of the solution volume in the subsequent experiments. The meander sensor is calibrated with absolute methanol solutions of 0.2 μL, 0.4 μL, 0.6 μL, and 0.8 μL, which laid flat on the measurement end to observe the variation of the transmission coefficient S_{21}, and the test results are shown in Fig. 10. As can be seen from the graph, the offset effect becomes worse as the liquid increases. This is due to the fact that when the volume of microfluidics increases, the channel capacitance changes

Table 2. Comparison table of minimum measurement volume for different sensors

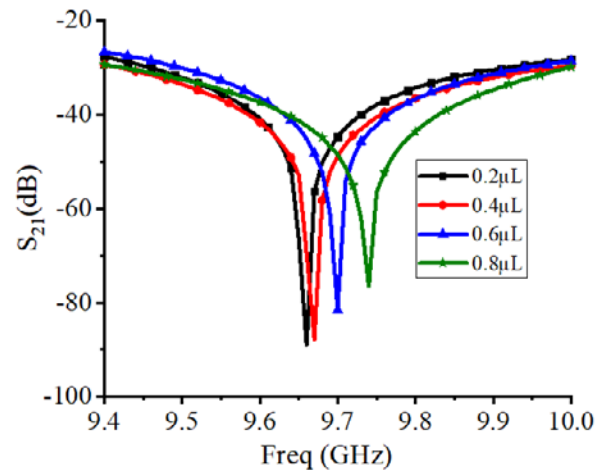|	Minimum Measurement Volume
Song [17]	<28 μL
Liu [29]	160 nL
Lan [32]	10 μL
This paper	0.4 μL

Figure 10. Effect of microfluidics volume on meander sensor.

accordingly, and thus the meander branch senses the change in liquid volume better, resulting in a larger difference in transmission between the two branches and a poorer offset effect. When the solution volume is 0.2 μL, as well as 0.4 μL, it is observed that the sensors' offset effect do not change significantly. However, the meander test branch is not completely covered by fluid if the solution volume is below 0.4 μL, so that the transmission coefficient S_{21} variation ΔS_{21} detected by the meander sensor is less than the true value. Therefore, the volume of microfluidics should be controlled in the subsequent experiment to reduce the error. The minimum volume of fluid that ensures that the microfluidics can spread over the meander test branch of the meander sensor is 0.4 μL (Table 2). In order to reduce the volume of the microfluidics measured, the design of reducing the meander line width can be further explored.

The reagent test of two sensors

After calibrating both sensors with 0.4 μL absolute methanol solution ($x_M = 1.0$), the $(S_{21})_{x_M=1.0}$ values of both sensors are obtained. The material under reference branch remains unchanged, and the material under test branch is replaced with methanol–ethanol mixture with a molar fraction of 0.9 to obtain the test values $(S_{21})_{x_M=0.9}$ of the two sensors. The parameters M and U are found by substituting $(S_{21})_{x_M=1.0}$ and $(S_{21})_{x_M=0.9}$ into Equations (4) and (6), respectively, where $\varepsilon_{x_M=0.9}$ and $\varepsilon_{x_M=1.0}$ are obtained by calculation in the literature [16]. The methanol–ethanol mixture with different molar fractions ($x_M = 0.0 \sim 0.8$) is changed at the test branch. The complex permittivity ε_{x_M} ($\varepsilon_{x_M} = \varepsilon' - j\varepsilon''$) of the methanol–ethanol mixture at different molar fractions is obtained

As shown in Fig. 11, the complex permittivity measured by the two sensors after calibration with mixture solution in literature is close to the reference value. Except the $x_M = 0.1$ group, the relative error of the meander sensor in measuring the complex permittivity of the methanol–ethanol mixture is less than 1% for all groups, which is smaller than that of straight sensor (less than 3%). In the simulation analysis of the methanol–ethanol mixture with a molar fraction of 0.1, the relative error is also larger than that of the other groups. The characteristics of the mixture solution at this molar fraction ($x_M = 0.1$) is different from other groups, or the error in the data from the reference compared in this group is larger than in the other groups. It can be seen from the experimental results that the meander sensor has a smaller test error and a higher test accuracy than straight sensor, which is more likely to detect the subtle changes of dielectric property from the precious and rare samples.

Conclusion

In order to improve the sensitivity of the cancellation-type sensor and apply it to small changes in the dielectric properties of biological sample such as cell, we proposed to introduce the meander line into the cancellation-type sensor. It is found that the meander transmission lines have a more concentrated field distribution at the meander section and are better able to sense changes in the dielectric properties of microfluids. A traditional straight sensor based on straight transmission lines is designed to compare and analyze the performance of the meander sensor. The relationship between the transmission coefficient of the two sensors and the dielectric properties of the microfluidics shows that the meander sensor can enlarge changes brought by microfluidics and thus make these weak changes more detectable. The simulation analysis shows that the meander sensor has a lower misclassification rate in determining methanol–ethanol mixtures with different molar fractions. Experiments show that the meander sensor is more accurate and the relative error is less than 1% in measuring the complex permittivity of unknown microfluidics. In addition, the offset effect of sensor after calibrating with an adjustable cavity is improved by more than 9 dB compared with that of previous research. Therefore, the meander sensor can be used for the test of weak dielectric parameter changes in microfluidics such as viruses in next work.

Competing interests. The authors declare that they have no known competing financial interests or personal relationships that could have appeared to influence the work reported in this paper.
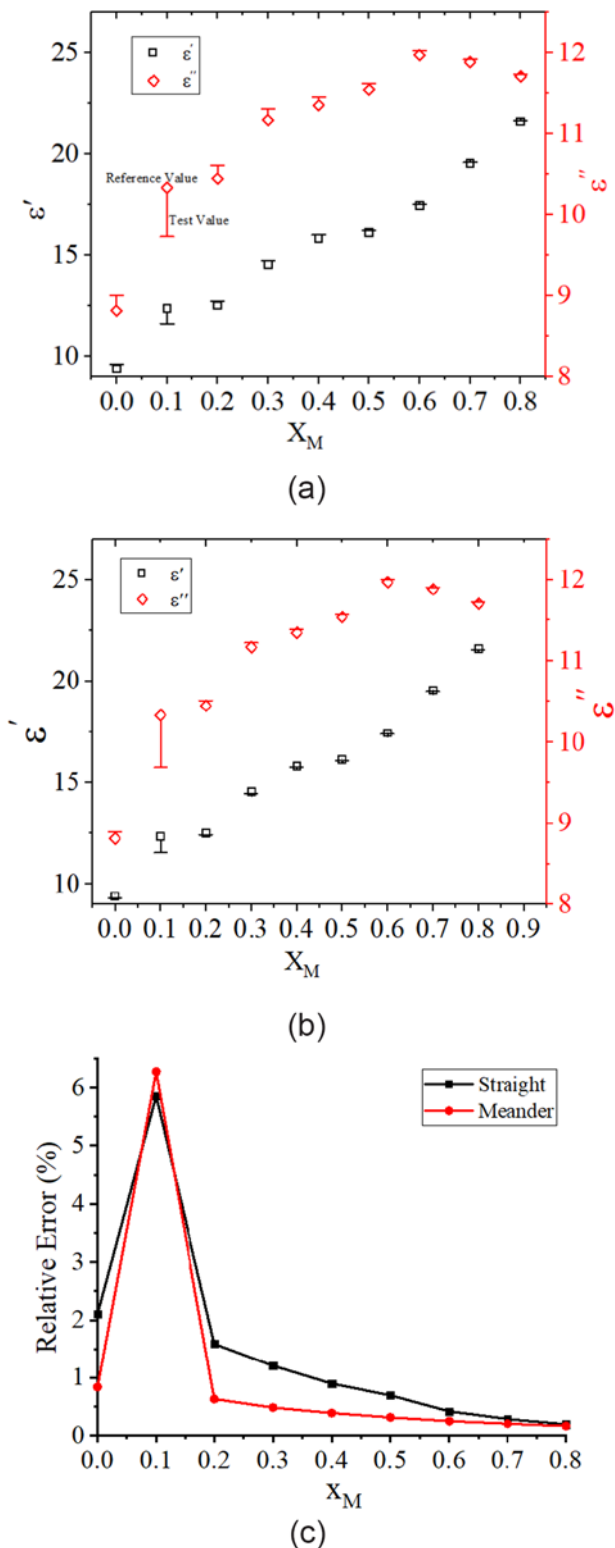
Figure 11. The complex permittivity of mixture from test and reference. (a) The test results of straight sensor. (b) The test results of meander sensor. (c) Comparison of the relative error measured by two sensors.

by substituting the measured ΔS_{21} into Equations (4) and (6). The complex permittivity measured by the two sensors is compared with the reference values to obtain Fig. 11.

References

1. **Hesabgar SM, Sadeghi-Naini A, Czarnota G and Samani A** (2017) Dielectric properties of the normal and malignant breast tissues in xenograft mice at low frequencies (100 Hz-1 mHz). *Measurement* **105**, 56–65.
2. **Shahzad A, Clausing D, Prakash P, Dennedy MC and O'Halloran M** (2017) Broadband dielectric properties of adrenal gland for accurate anatomical modelling in medical applications. In *19th International Conference on Electromagnetics in Advanced Applications (ICEAA)*, 1465–1468.
3. **Amin B, Elahi MA, Shahzad A, Porter E and Halloran M** (2019) A review of the dielectric properties of the bone for low frequency medical technologies. *Biomedical Physics & Engineering Express* **5**, 022001.

4. **Ng CL and Reaz MB** (2019) Evolution of a capacitive electromyography contactless biosensor: Design and modelling techniques. *Measurement* **145**, 460–471.

5. **Abdullah S, Tonello S, Borghetti M, Sardini E and Serpelloni M** (2019) Potentiostats for protein biosensing: Design considerations and analysis on measurement characteristics. *Journal of Sensors* **2019**, 20.

6. **Mansouri S, Alhadidi T and Ben Azouz M** (2020) Breast cancer detection using low-frequency bioimpedance device. *Breast Cancer-Targets and Therapy* **12**, 109–116.

7. **Liz BS** (2019) A 3-bit fully inkjet-printed flexible chipless RFID for wireless concentration measurements of liquid solutions. *Sensors and Actuators A: Physical* **299**, 111581.

8. **Vasimalla Y and Singh L** (2023) Design and analysis of planar waveguide-based SPR sensor for formalin detection using Ag-Chloride-BP structure. *IEEE Transactions on NanoBioscience* **22**(2), 365–374.

9. **Hemamalini V, Anand L, Nachiyappan S, Geeitha S, Motupalli VR, Kumar R, Ahilan A and Rajesh M** (2022) Integrating bio medical sensors in detecting hidden signatures of COVID-19 with artificial intelligence. *Measurement: Journal of the International Measurement Confederation* **194**, 111054.

10. **Priyadarshani KN, Singh S and Mohammed MKA** (2022) Gate-all-around junctionless fet based label-free dielectric/charge modulation detection of SARS-COV-2 virus. *RSC Advances* **12**(15), 9202–9209.

11. **Stelson AC, Liu M, Little CAE , Long CJ, Orloff ND, Stephanopoulos N and Booth JC** (2019) Label-free detection of conformational changes in switchable DNA nanostructures with microwave microfluidics . *Nature Communications* **10**(1), 1174.

12. **Sadighbayan D, Minhas-Khan A and Ghafar-Zadeh E** (2022) Laser-induced graphene-functionalized field-effect transistor-based biosensing: A potent candidate for COVID-19 detection. *IEEE Transactions on NanoBioscience* **21**(2), 232–245.

13. **Kozhevnikov A** (2010) Wideband radio-frequency device for measurements of dielectric properties of small volumes of liquids . *Measurement Science and Technology* **21**(4), 043001.

14. **Pourghorban Saghati A, Batra JS, Kameoka J and Entesari K** (2017) A metamaterial-inspired wideband microwave interferometry sensor for dielectric spectroscopy of liquid chemicals. *IEEE Transactions on Microwave Theory and Techniques* **65**, 2558–2571.

15. **Lobato-Morales H, Corona A, Olvera-Cervantes JL, Chavez-Perez RA and Medina-Monroy JL** (2014) Wireless sensing of complex dielectric permittivity of liquids based on the RFID . *IEEE Transactions on Microwave Theory and Techniques* **62**, 2160–2167.

16. **Mashimo S, Umehara T and Redlin H** (1991) Structures of water and primary alcohol studied by microwave dielectric analyses. *Journal of Chemical Physics* **95**(9), 6257–6260.

17. **Cole KS and Cole RH** (1941) Dispersion and absorption in dielectrics I. Alternating current characteristics. *The Journal of Chemical Physics* **9**(4), 341–351.

18. **Song CR and Wang PS** (2008) IEEE. On-chip cancellation of parasitic effects for dielectric permittivity measurement. In *2008 IEEE MTT-S International Microwave Symposium Digest*, vols 1–4. New York: IEEE, 1720–1723.

19. **Song CR and Wang PS** (2009) A radio frequency device for measurement of minute dielectric property changes in microfluidic channels. *Applied Physics Letters* **94**(2), 3.

20. **Yang Y, Zhang HQ, Zhu JJ, Wang GY, Tzeng T-R, Xuan XC, Huang K and Wang PS** (2010) Distinguishing the viability of a single yeast cell with an ultra-sensitive radio frequency sensor. *Lab on a Chip* **10**(5), 553–555.

21. **Liu WN, Zhang JJ and Huang KM** (2022) Wideband microwave interferometry sensor with improved sensitivity for measuring minute variations in dielectric properties of chemical liquids in microfluidic channels. *Measurement* **189**, 14.

22. **Wang HY, Liu XQ, Xiong R and Huan Z** (2021) Adjustable cancellation type high sensitivity radio frequency sensor. *Measurement* **168**, 6.

23. **Liu WN, Zhang JJ and Xu L** (2021) A transmission line sensor with sensitivity improved for detection of ionic concentration in microfluidic channel. *IEEE Sensors Journal* **21**(21), 24066–24074.

24. **Cui Y, He Y and Wang P** (2014) A quadrature-based tunable radio-frequency sensor for the detection and analysis of aqueous solutions. *IEEE Microwave and Wireless Components Letters* **24**(7), 490–492.

25. **Cui Y and Wang P** (2014) The design and operation of ultra-sensitive and tunable radio-frequency interferometers. *IEEE Transactions on Microwave Theory and Techniques* **62**(12), 3172–3182.

26. **Chen Z, Shao YZ and Wang PS** (2015) Resonator- and filter-induced slow waves for high-sensitivity rf interferometer operations. *IEEE Sensors Journal* **15**(5), 2993–2999.

27. **Meyne N, Müller-Wichards W, Trieu HK and Jacob AF** (2014) Quasi-lumped coplanar transmission-line sensors for broadband liquid characterization. In *2014 44th European Microwave Conference*, 687–690.

28. **Haase NMN, Fuge G, Trieu HK, Zeng A-P and Jacob AF** (2015) Miniaturized transmission-line sensor for broadband dielectric characterization of biological liquids and cell suspensions. *IEEE Transactions on Microwave Theory and Techniques* **63**(10), 3026–3033.

29. **Turgul V and Kale I** (2018) Permittivity extraction of glucose solutions through artificial neural networks and non-invasive microwave glucose sensing. *Sensors and Actuators A: Physical* **277**, 65–72.

30. **Liu XQ, Zou H, Zhu B, Lin H and Wang HY** (2021) An ultra-sensitivity cancellation type sensor based on microstrip meander-line. In *3rd IEEE International Conference on Circuits and Systems, ICCS 2021*, October 30, 2021–November 2, 2021, 59–63.

31. **Liu WN** (2016) A novel technology for measurements of dielectric properties of extremely small volumes of liquids. *International Journal of Antennas and Propagation* **2016**, 5.

32. **Lan K, Zou H, Qiu WH and Wang HY** (2018) High sensitivity off-set sensor based on coplanar waveguide. *Foreign Electronic Measurement Technology* **37**(09), 18–21.
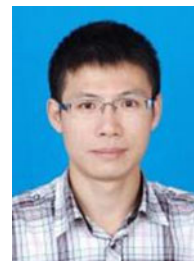
Huan Zou received her Ph.D. degree in physical electronics from the University of Electronic Science and Technology of China (UESTC), Chengdu, China, in 2011. She was a visiting scholar at the School of Electrical and Computer Engineering at Clemson University in the United States from 2007 to 2010. Her current research interests include microwave/millimeter wave devices and circuit design.

Yiyun Wang received the B.S. degree in 2022 from Zhengzhou University. She is currently working toward the M.S. degree in the University of Electronic Science and Technology of China (UESTC). Her current research interests include microwave/millimeter wave devices and circuit design.

Xiaoqin Liu received the M.S. degree in 2022 from the University of Electronic Science and Technology of China. Her current research interests include microwave/millimeter wave devices and circuit design.

Haiyang Wang received his Ph.D degree in physical electronics from the University of Electronic Science and Technology of China (UESTC), Chengdu, China, in 2009. His current research interests include high-power microwave electromagnetic effects and electromagnetic protection.